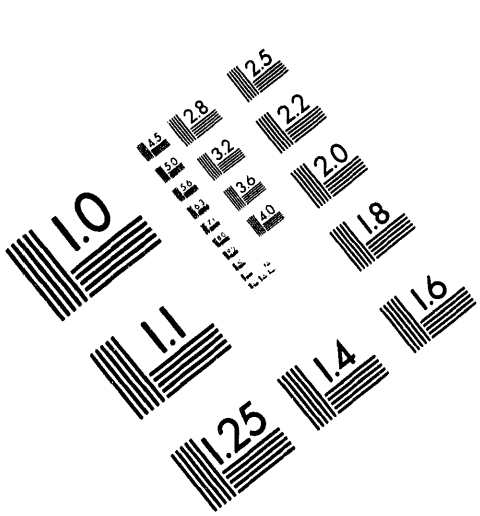

Association for Information and Image Management
1100 Wayne Avenue, Suite 1100
Silver Spring, Maryland 20910
301/587-8202

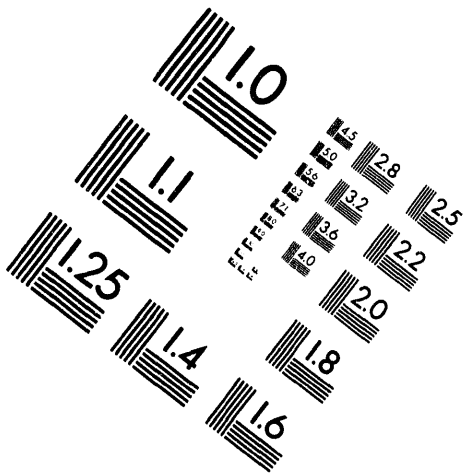

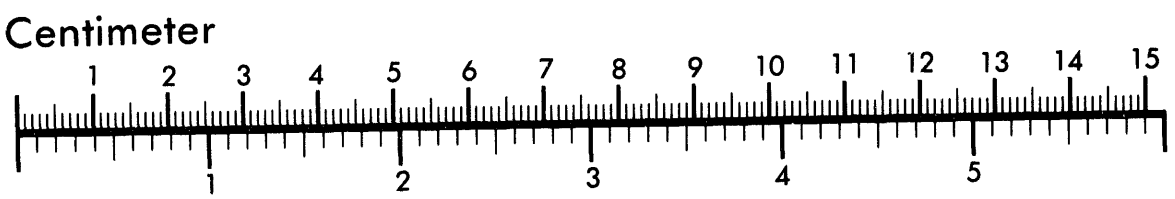

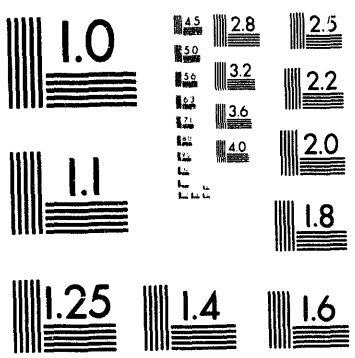

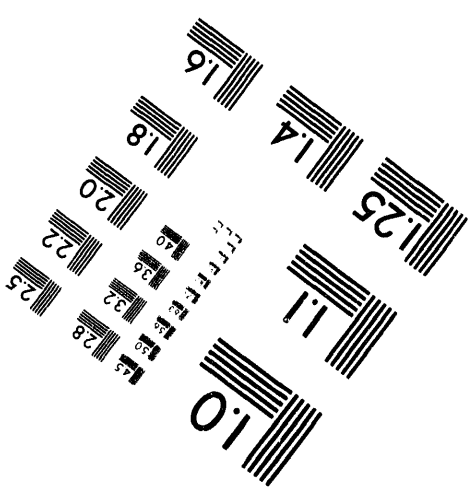

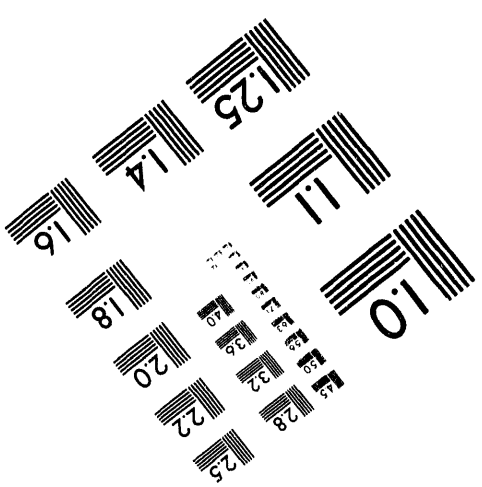

MANUFACTURED TO AIIM STANDARDS
BY APPLIED IMAGE, INC.

1 of 1

PPPL-CFP-3083
Conf-940630--20

RADIATION SHIELDING FOR TFTR DT DIAGNOSTICS

L. P. Ku, D. W. Johnson, and S. L. Liew
Princeton Plasma Physics Laboratory
P. O. Box 451, Princeton, NJ 08543-0451
(609)243-2598

ABSTRACT

We illustrate the designs of radiation shielding for the TFTR DT diagnostics using the ACX and TVTS systems as specific examples. The main emphasis here is on the radiation transport analyses carried out in support of the designs. Initial results from the DT operation indicate that the diagnostics have been functioning as anticipated and the shielding designs are satisfactory.

The experience accumulated in the shielding design for the TFTR DT diagnostics should be useful and applicable to future devices, such as TPX and ITER, where many similar diagnostic systems are expected to be used.

I. INTRODUCTION

The Tokamak Fusion Test Reactor (TFTR) has entered the deuterium-tritium operating mode to study isotopic and alpha particle effects [1]. Large arrays of diagnostics are employed to measure the plasma properties and fusion product characteristics. Many of the detectors used, especially those for the spectroscopy, are sensitive to nuclear radiation. With the neutron production rate expected to exceed 10^{18} n/s routinely, these detectors, if left unshielded, would give rise to unacceptably high background noise levels, leading to possible pulse pileup, spectrum distortion, and resolution degradation.

To prepare for the increased radiation during DT operations, measures were taken to limit the radiation induced effects. These included replacing sensitive components with radiation resistant ones, relocating detectors to areas where either some shielding already existed or the expected radiation levels would be lower, and designing new radiation shields. For example, plastic fibers were replaced with quartz fibers to reduce radiation induced fluorescence and opacity. The Charge Exchange Recombination system has been moved into the hot cell using the 5-feet concrete wall as the primary shielding. New shielding has been installed for the Thomson scattering (TVTS), alpha charge exchange analyzer (ACX) and VUV Survey Spectrometer systems, among others. A summary of the diagnostics preparation for the TFTR DT operation may be found in [2].

In this paper, we summarize the approach taken for designing the new radiation shields with emphasis on the radiation analyses carried out in support of the design, using TVTS and ACX systems as specific examples. These two systems have quite different radiation environment at their respective locations and the detector response characteristics are different as well.

II. METHOD AND APPROACH[3]

Before proceeding with the mechanical design of a shield, we evaluate three essential elements for a diagnostic system: (1) the expected neutron and gamma-ray fluxes at the detector (in energy, space and angle), (2) the expected detector response to radiation (considered as noise), (3) the desirable signal-to-noise ratio. From the evaluation, we derive radiation attenuation factors required and find means to achieve the attenuation. Typically, one-dimensional radiation transport calculations would be carried out to optimize the attenuation effectiveness of various material combinations, including the availability, cost and safety in the consideration. The thicknesses determined from the optimization study are compared with the available space surrounding the diagnostics in question and a preliminary mechanical design is carried out to find out the required structural support. Penetrations that have to go through the shield are laid out, and alterations to accommodate local geometrical constraints are made. More rigorous radiation transport analyses, frequently involving multi-dimensional calculations with semi-realistic geometrical configurations, are carried out to ensure the design meets the required signal-to-noise level. Often, a few iterations are needed before the final design is completed and construction can proceed.

III. DESIGN OF ACX SHIELDING

A sketch of the ACX diagnostic system is given in Figure 1. The system is located about 8 m from the center of the machine on the north direction next to the pellet injector. A pipe, 3.175 cm in diameter, is connected to the vacuum vessel, allowing charge-exchanged alphas to flow into the analyzer. The detector is made of CsI scintillators, which are located at a ~90° angle from the line-of-sight of the connecting pipe.

A. Evaluation of Radiation Fields at the Detector

The neutron and gamma-ray fluxes at the ACX were determined using the semi-empirical algorithm given in [4]. In this algorithm, the fast neutron flux (E>2 MeV) was derived from dose equivalent measurements outside the north concrete wall behind the ACX. The slow neutron and photon fluxes were derived from transport calculations with the model adjusted to make results consistent with the dose equivalent measurements. Using this semi-empirical method, we were able to take into proper account the complex ex-tokamak structures in the shielding design.

B. Evaluation of Detector Response to Radiation

During testing with high power DD discharges, significant noise contributions from neutrons and gamma-rays were observed in the CsI scintillators and in the photomultipliers as well. The photomultipliers were moved to the basement as a result. The coupling to the light output from the scintillators was accomplished by the optical fibers.

We considered three nuclear energy dissipation processes which could lead to excitations in CsI, hence the unwanted scintillation: (1) slowing down of recoil electrons from the gamma-ray interactions, (2) slowing down of alphas from the (n,α) reactions, and (3) slowing down of protons from the (n,p) reactions. The amount of nuclear energy that is converted to the light energy is the product of (1) the energy of the recoil charged particle, (2) the amount of this energy dissipated in the CsI crystal, and (3) the conversion efficiency of the charged particle energy dissipated in the crystal to light energy. Without shielding, the electron energy deposited is ~2 J per kg of CsI for a 30 MJ DT pulse. For alphas and protons, the average recoil energies from the neutron interaction are ~10 MeV and 3 MeV, respectively. The large recoil energy of the alphas is due to the facts that the (n,α) reaction for both Cs and I are exoergic with Q=4.4 MeV and that the reaction cross section becomes appreciable only for neutron energies >10 MeV. Combining with the reaction rates, we obtain, for an unshielded CsI, the energy depositions of 1.5×10^{-4} and 4×10^{-3} J/kg per 30 MJ DT discharge, from recoil alphas and protons.

The ranges of all the recoiled charged particles are much greater than the 8 μm CsI phosphor used (e.g., 500 μm for 500 keV electron, 200 μm for 3 MeV protons, and 100 μm for 10 MeV alphas). Hence, the fraction of the charged particle energy absorbed in the CsI scintillator is approximately inversely proportional to the range. Furthermore, the effects due to back scattering and in-leakage of particles from surrounding materials are most pronounced for the electrons. Thus, we conclude that it is the gamma-ray sensitivity that determines the shield thickness.

C. Determination of Shield Thickness

From the detector response observed during DD discharges, it was determined that a shield which provides a factor of 50-100 reduction would be appropriate during DT. Figure 2 shows the specific energy deposition in CsI as a function of polyethylene (with 5% w/o boration) thickness for two-layered polyethylene (PE) and lead (Pb) shield obtained from one-dimensional ANISN [5] calculations. Although other materials can be used, we chose PE and Pb based on the past experience and low cost of Pb. We have used, in the calculations, a cosine angular distribution for multiscattered sub-MeV neutrons, but a forward-peaking source for neutrons with energies near 14 MeV. The figure is therefore more appropriate for the front shield facing the tokamak. From the figure, we found the minimum shield thickness to achieve the 100-fold attenuation: 0.15 m PE plus 0.10 m Pb.

D. Effects of Penetrations

Since the scintillators are not in the direct line-of-sight of penetrations, the increase in the scintillator response, R, may be estimated by [6]

$$R = k \cdot C \cdot S / A, \qquad (1)$$

where k is the scattering factor for neutrons or gamma-rays in an enclosed Pb/PE cell, C is the conversion factor from flux to detector response, S is the total neutrons or photons entering the shield box and A is the interior surface area of the shield.

The scattering factor is related to the albedo of the shield material. Using an albedo of 0.9 and assuming that all the neutrons incident on the mouth of the penetration would enter the shield box, we obtained an increase in the specific energy deposition of a few percent.

E. Other Considerations.

The Pb was secured into place using the existing frames. The PE plates were bolted outside and covered with a cement board for fire safety. Calculations of

bending and overturning moments as well as the stress due to both the gravitation and seismic loads indicated that the mechanical design was satisfactory. The final design is shown schematically in Fig. 1.

IV. DESIGN OF TVTS SHIELDING

Figure 3 shows the layout of the TVTS system. The detector and laser generator are located in the basement about 12 m from the center of the machine on the north-east corner. The laser beams are transmitted via fiber optics through penetrations in the test cell floor and machine substructure. The detector is a CCD camera.

A. Evaluation of Radiation Fields at the Detector

To arrive at the radiation levels at the detector location, two source components would have to be considered: (1) radiation penetrating through the test cell floor, and (2) radiation leaking from various penetrations in the substructure.

The neutron transport model constructed for (1) above was a one-dimensional spherical representation of the test cell, with material densities adjusted so that it would yield the same results as a three-dimensional model would as discussed in [4]. An effective floor thickness was used to include the effects of slant incident of the radiation onto the floor. This effective thickness was found by equating the basement fluxes calculated from the one-dimensional model to those from a two-dimensional test cell model [7].

The transport model constructed for (2) was a spherical representation of the basement. A stainless steel center core, 5 m in radius, was modeled to represent the diagnostics underneath the machine. An outer concrete shell, 0.6 m in thickness, was modeled to represent the basement floor, ceiling and walls. Neutrons were injected into this basement model with the intensity adjusted so that the dose equivalents calculated at the radiation monitoring locations were equal to those measured. It was found that the 'efficiency' for fast neutrons streaming into the basement through open penetrations was $\sim 5\times10^{-5}$. The neutron and photon fluxes calculated at the TVTS detector location were 10^8 n/cm^2 and 3×10^8 γ/cm^2, respectively, per 30 MJ DT fusion. The corresponding absorbed dose in Si was about 100 mrad.

B. Evaluation of Detector Response to Radiation

The CCD sensitivities to radiation may be measured by the absorbed dose in silicon (ionization effects) and neutron fluxes (dark current spikes). Studies of detector sensitivity to radiation in TFTR were carried out during high power DD discharges ($> 5\times10^{15}$ n/s) to establish the acceptable limits on the flux levels. It was determined that, for the purpose of shielding design, the calculated flux levels should be limited to $<10^7$ n/cm^2-s and the silicon dose rate to <1 mrad/s at the CCD camera.

C. Determination of Shield Thickness

Using the technique outlined in Section III, we determined that a 0.1 m layer of PE (5%B) followed by 0.1 m Pb should be sufficient to meet the design goal for the side shield. The front end of the shield box cannot be fully closed, however. Fortunately, the lenses used to focus the lights have a total thickness of 0.25 m, and about half of which are the lead glasses, so that the CCD sees little streaming radiation directly from the front opening. To quantify the front-end effects, a two-dimensional R-Z model was constructed and transport calculations were carried out using the DORT [8] discrete-ordinates code. The detector assembly was modeled as a cylinder with all components assumed to be azimuthally symmetric. Figure 4 shows the model and an example of the neutron flux contours. It was concluded that the perturbation due to the front end opening would not be significant so long as we maintained a shield with length >0.5 m.

D. Other Considerations

The shield materials were held in place using aluminum grid structures and anchors. The total weight was about 30,000 lbs. A section of the back shield was flexibly designed so that it may be swung open to allow rapid access to the detector. As before, a cement board was attached on the outside as a fire safety measure.

V. SUMMARY AND CONCLUSIONS

In preparation for DT operation, where the neutron yield was expected to increase by two orders of magnitude compared to the DD operation, detector sensitivities to radiation were reviewed and shields required to limit noise levels were installed. We selected two systems, the ACX and TVTS, to illustrate our approach to the shield design. We made an effort to identify, as realistically as possible, the local neutron and photon fluxes. One-dimensional optimization studies were then carried out using a direct iterative technique to find out the best combination of materials and thickness. Most frequently, we chose a PE and Pb combination due to its effectiveness, cost, and availability. Multi-dimensional radiation transport analyses were performed following the preliminary design to ensure the design goal could be met in the existence of design perturbations. Initial results from the DT operation indicate that the diagnostics have

been functioning as anticipated and the shielding designs are satisfactory.

ACKNOWLEDGMENTS

This work was supported by US Department of Energy Contract DE-AC02-76-CHO-3073.

REFERENCES

1. R. J. Hawryluk, H. Adler, P. Alling, et al., "Confinement and Heating of a Deuterium-Tritium Plasma," PPPL-2977, Princeton Plasma Physics Laboratory (1994).

2. D. Johnson, K. Hill, L. P. Ku, et al., "Diagnostic Preparations for TFTR DT Phase," *Proc. APS Division of Plasma Physics*, St. Louis Mo, November 1-5 (1993).

3. S. L. Liew and L. P. Ku, "Radiation Shielding Aspects of the TFTR Diagnostics," *Proc. 12th Symposium on Fusion Engineering, Monterey Ca*, October 12-16 (1987).

4. L. P. Ku and S. L. Liew, "A Semi-Empirical Algorithm for Determining Radiation Field Characteristics in TFTR," *Proc. 8th International Conference on Radiation Shielding*, Arlington, Tx, April 25-28 (1994).

5. W. W. Engle, Jr., "The User's Manual for ANISN: A One-Dimensional Discrete Ordinates Transport Code with Anisotropic Scattering," K-1694 Oak Ridge National Laboratory (1967).

6. L. P. Ku and J. Kolibal, "A Study of Scattered Fusion Neutron Distributions in a Bounded Concrete Cell," *Trans, Am. Nucl. Soc.*, 46, 635 (1984)

7. J. Kolibal and L. P. Ku, "Prompt Radiation Environment for the TFTR Q=1 Demonstration," *Proc. 10th Symposium on Fusion Engineering*, Philadelphia. Pa, Oct 10-14 (1983).

8. W. A. Rhoades and R. L. Childs, "The DORT Two-Dimensional Discrete Ordinates Transport Code," Nucl. Sci. & Eng., 99, 88 (1988).

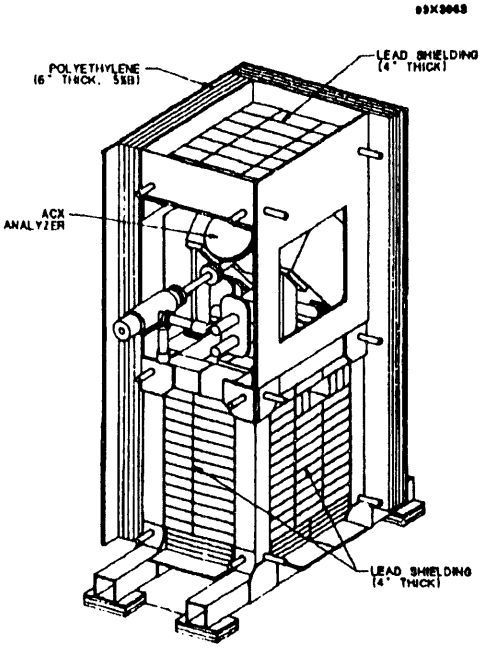

Fig 1. Schematic showing the ACX detector assembly and shielding.

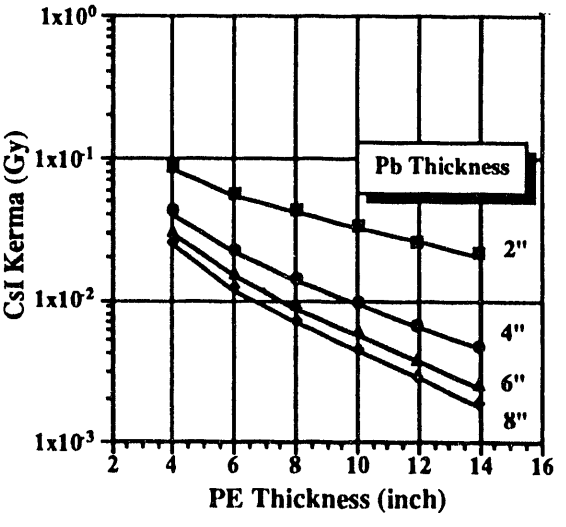

Fig 2. Attenuation of energy deposition in CsI as function of polyethylene(5%B) and Pb thicknesses.

DISCLAIMER

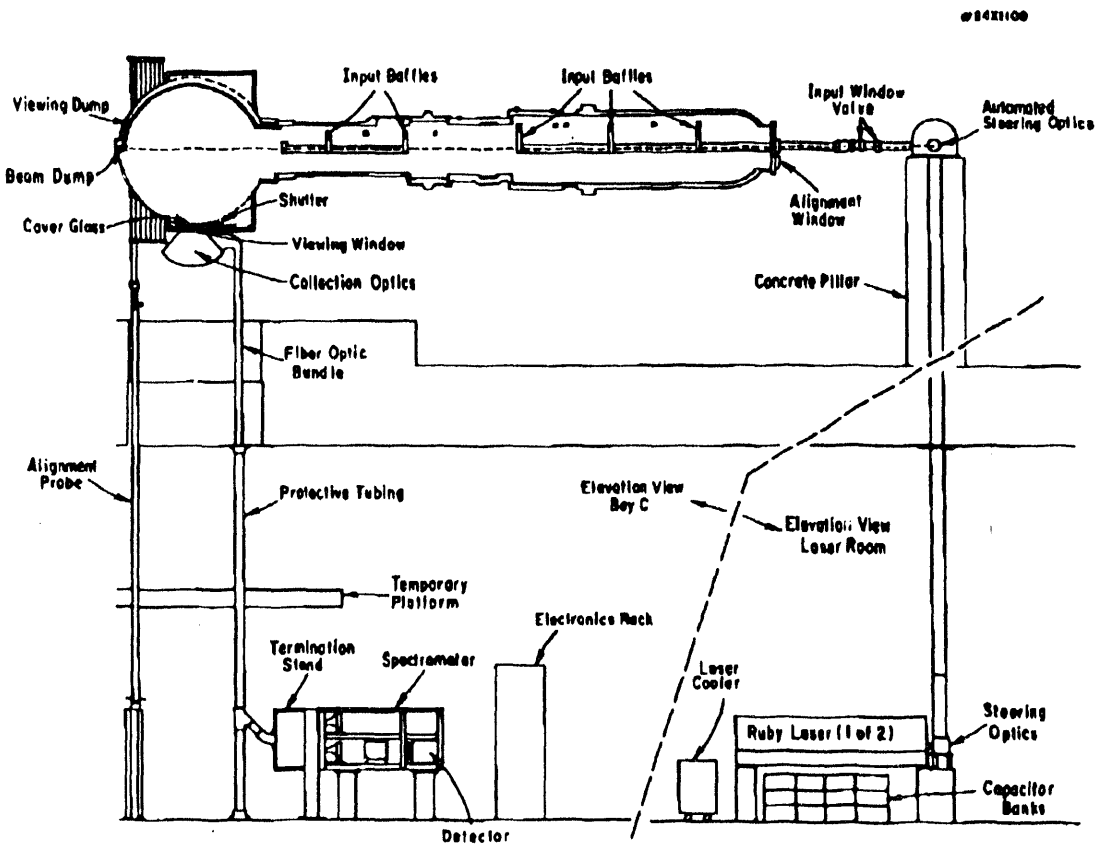

Fig. 3 Schematic showing the TVTS system and the detector location relative to the vacuum vessel.

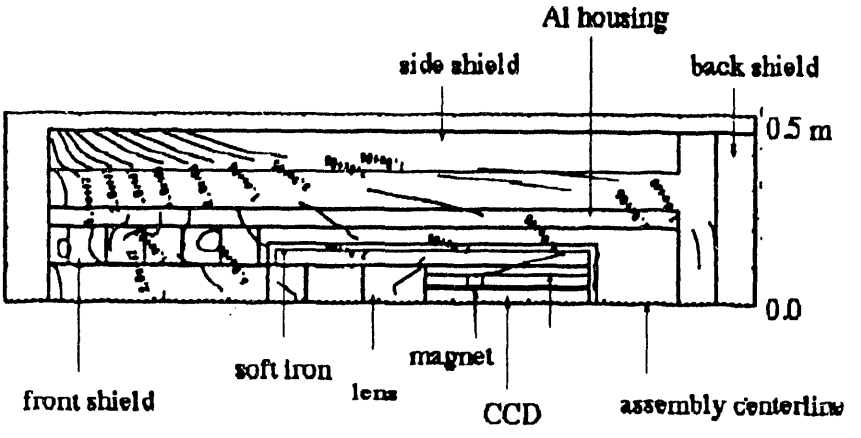

Fig. 4 Schematic showing the axi-symmetric R-Z model of the TVTS detector assembly for radiation transport calculations. Neutron flux contours are also shown for neutrons incident on the front surface of the shield.

DATE
FILMED
8/15/94

END